ELSEVIER

Journal of Nuclear Materials 277 (2000) 130–142

journal of nuclear materials

www.elsevier.nl/locate/jnucmat

Comparison of hydrogen gas–, atom– and ion–metal interactions

O.V. Ogorodnikova

Commissariat à *l'Energie Atomique, CEA/Saclay, DRN/DMT/SERMA, F-91191 Gif-sur-Yvette, France*

Received 19 May 1999; accepted 5 August 1999

Abstract

In the first part of the paper, we describe in more detail the dissociative chemisorption model, presented by Wang for the gas–metal interaction and then developed by Pick and Sonnenberg for the atom–metal interaction, in order to show the important factors which were not taken into account by previous authors. One of these factors is the initial sticking coefficient s_0 which can be less than unity even for a clean surface and can strongly influence the plasma-driven permeation and inventory. Then, we extend the dissociative chemisorption model on the case of the interaction of hydrogen molecular gas and fast hydrogen atoms with a multi-layer metal, and we verify the validity of the model by comparison of experimental data with calculations. Although in recent theoretical papers [Richards; Pisarev and Ogorodnikova] it was shown that Baskes' model has an error, many authors apply Baskes' recombination coefficient for their calculations till now. Experimental measurements show that the plasma-driven permeation and inventory are a function of the sticking coefficient which is very sensitive to any surface contamination that is in contradiction with Baskes' model. Finally, on the basis of the dissociative chemisorption model, the assessment of the plasma-driven permeation through martensitic steel MANET covered by some plasma-facing metals (copper, beryllium and beryllium oxide) is presented. We show that the experimental data of hydrogen isotope permeation and inventory measured for the gas–metal interaction cannot be applied for the plasma-driven permeation and inventory. The analysis of the existing database of the sticking coefficient s updates those estimates for endothermic metals which can be applied for the fusion reactor.

Introduction

Understanding the hydrogen escape from the metal is significant for many applications, especially for prediction of the magnitude of hydrogen desorption, permeation and inventory for materials used in fusion reactors. Wang [1] was the first who presented the dissociative chemisorption model to describe kinetics of elementary processes near the interface between hydrogen gas and metal. The question of hydrogen-metal interaction was studied in detail by Waelbroeck [2], Livshitz [3], and Baskes [4]. Later, these models were improved by Pick and Sonnenberg [5] and Richards [6].

In part I of the paper, the careful description of the dissociative chemisorption model is given to emphasize some details which did not catch attention in the original papers. The presented fitting of analytical expressions can be useful for evaluation of the gas– and plasma-driven uptake and permeation in both the diffusion-limited and the surface-limited regimes.

In part II, the comparison of experimental data with analytical calculations of the permeation and uptake for several endothermic metals in contact with deuterium gas, atoms or ions is performed. As it will be shown below, experimental and calculated results are in excellent agreement that indicates the validity of the model. On the other hand, the model proposed by Baskes and often used for the description of the plasma-driven permeation, leads to the discrepancy with experimental observations.

In part III, on the ground of the dissociative chemisorption model and existing database of the sticking

E-mail address: olga@soleil.serma.cea.fr (O.V. Ogorodnikova).

0022-3115/00/$ - see front matter
PII: S0022-3115(99)00206-8

factor, the assessment of the gas- and atom-driven permeation of tritium through multi-layer metal of interest in controlled fusion is presented.

Part I. Model

1. Interaction of molecular gas with metal

1.1. Description of the fluxes near the hydrogen–metal interface

The hydrogen–solid interaction is usually described by the potential diagram shown schematically in Fig. 1 [1–7]. The mechanisms of penetration of hydrogen molecular gas and hydrogen atoms or ions into the metal are different. In order to penetrate into the bulk, a molecule needs to dissociate into two atoms. For many cases, this process is thermally activated. On the other hand, fast hydrogen atoms or ions penetrate immediately from the plasma into the bulk of the metal without being chemisorbed on the surface.

Let us consider the interaction of molecular hydrogen gas with metal membrane of thickness L. According to the kinetic theory of gases, the flux of gas molecules to the surface is $I_0 = p\mu$ (molecules/m^2 s), where p is the gas pressure and $\mu = 1/\sqrt{2\pi mkT}$ (m is the gas molecular mass, T the temperature, k is Boltzmann's constant). In order to describe the fluxes of hydrogen near the metal surface, two basic types of sites for hydrogen atoms are considered: chemisorption sites on the metal surface with concentration n (atoms/m^2) and absorption sites in the bulk of metal with concentration u (atoms/m^3). Let us introduce n_m and u_m which are the maximum available concentrations on the surface and in the bulk, respectively, ν_c (s^{-1}) and ν_s (s^{-1}) which are an attempt frequency for hydrogen atom jumps between positions in the chemisorption state on the surface and in the solution state in the bulk of the metal, respectively, and λ (m) which is the jump distance between interstitial sites in the lattice. The maximum available hydrogen concentration in the bulk u_m is assumed to be equal to the atomic density of the metal host N multiplied by the number of interstitial solution sites $u_m = Nz$ ($z = 4$ for fcc and $z = 6$ for bcc). The atomic areal density of chemisorption sites is roughly assumed to be $n_m = \sqrt[3]{u_m^2}$.

The following fluxes to and from the surface are represented in Fig. 1:

(1) The flux of particles sticking to the surface from the gas is $J_1 = sI_0(1 - n/n_m)^2$ (molecules/m^2 s); $s = s_0 \exp(-2E_c/kT)$ is the so-called sticking coefficient, where s_0 is the sticking coefficient at low surface coverage and non-activated sorption and E_c is the activation energy for chemisorption.

(2) The desorption flux is given by $J_2 = k_2 n^2$ (molecules/m^{2}s), $k_2 = \nu_c \lambda^2 \exp(-2(E_c - Q_c)/kT)$, where Q_c is the heat of chemisorption.

(3) The flux from the chemisorption site to the solution site is $J_3 = k_3 n(1 - u/u_m)$ (atoms/m^2 s), $k_3 = \nu_c \exp(-(E_s - Q_c)/kT)$, where E_s is the activation energy for transitions from the surface to the bulk.

(4) The reverse flux from the bulk to the surface is given by $J_4 = k_4 u(1 - n/n_m)$ (atoms/m^2 s), $k_4 = \nu_s \lambda \exp(-(E_s - Q_s)/kT)$.

Pick and Sonnenberg [5] applied the similar description of fluxes J_i near the gas–metal interface using $N^{-1/3}$ (N is the metal density) instead of λ.

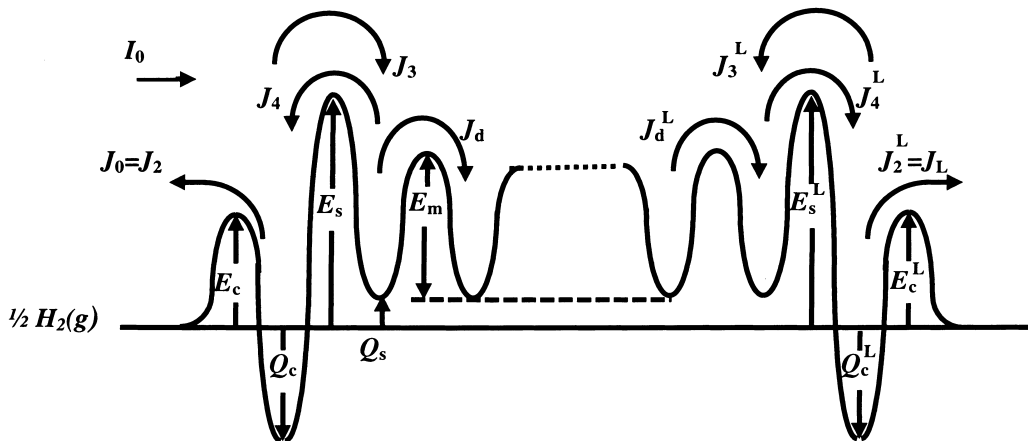

Fig. 1. Schematic energy diagram of hydrogen/metal interaction. E_c, Q_c, E_s, Q_s and E_m are the activation energies for dissociative chemisorption, the heat of chemisorption on the surface, the activation barrier for the jump from the chemisorption site on the surface to the absorption site in the bulk, the heat of solution and the activation energy for diffusion, respectively.

1.2. Inventory

At equilibrium the net of inflow and outflow is equal to zero:

$$-2k_2n^2 + 2I_0s(1 - n/n_m)^2 + k_4u(1 - n/n_m) - k_3n = 0, \quad (1)$$

$$-k_4u(1 - n/n_m) + k_3n = 0. \quad (2)$$

Here, it is assumed that hydrogen concentration in the bulk is much lower than the maximum available hydrogen concentration ($u \ll u_m$). These equations yield the following expressions for the hydrogen concentrations on the surface n and in the bulk u:

$$n/(1 - n/n_m) = \sqrt{sI_0/k_2}, \quad (3)$$

$$u = (k_3/k_4)\sqrt{sI_0/k_2}. \quad (4)$$

A similar expression for the bulk concentration, u, was obtained in [5] by Pick and Sonnenberg. At low surface coverage ($n \ll n_m$) Eqs. (3), (4) together with s, k_2, k_3, and k_4 yield the following expressions for n and u, respectively:

$$n_s = \exp(-Q_c/kT)\sqrt{s_0I_0/v_c\lambda^2}, \quad (5)$$

$$u_s = \exp(-Q_s/kT)\sqrt{s_0I_0/v_s\lambda^4}\sqrt{v_c/v_s}. \quad (6)$$

It is not surprising that both concentrations on the surface n and in the bulk u depend only on heats of chemisorption Q_c and solution Q_s, respectively, and are independent of activation barriers.

We assume that the lattice is undistorted up to the surface. In this case, v_c and v_s have the same order of magnitude ($v_c \approx v_s \approx 10^{13}$ s^{-1}) and, for simplification, we will consider $v_c = v_s = v$. Using this suggestion, Eq. (6) can be written as

$$u_s = \sqrt{s_0\mu/v\lambda^4}\exp(-Q_s/kT)\sqrt{p} = K_s\sqrt{p}, \quad (7)$$

where $K_s = \sqrt{s_0\mu/v\lambda^4}\exp(-Q_s/kT)$ is Sieverts' constant for the material. The relationship of the pre-exponential factor K_{s_0} of Sieverts' constant with v and λ is given by

$$v\lambda^4 = s_0\mu/K_{s_0}^2. \quad (8)$$

The diffusion pre-exponential factor can be presented as

$$D_0 = gv\lambda^2/6, \quad (9)$$

where g is the geometrical factor which is different for bcc and fcc metals [8]. Using together Eqs. (8) and (9), we can derive the sticking pre-factor for a clean metal surface

$$s_0 = (6D_0K_{s_0}^2\lambda^2/g\mu). \quad (10)$$

1.3. Recombination coefficient

The hydrogen release from the metal may be controlled by diffusion- or surface-limited processes such as adsorption and desorption. In order to provide a description of surface barrier effects, the knowledge of the recombination coefficient is required.

It is usually supposed that the rate of hydrogen thermodesorption from a surface is proportional to the square of the concentration of atoms chemisorbed on surface sites: $J_0 = J_2 = k_2n^2$ (molecules/m^2 s). However, to simplify the mathematical task, it is proposed that the desorption rate J_0 is proportional to the square of the bulk concentration u of hydrogen under the surface [9]. The proportionality coefficient was named the recombination coefficient:

$$K_r = J_0/u^2 \text{ (m}^4 \text{ molecules/atoms}^2 \text{ s)}. \quad (11)$$

Using Eq. (5) for n and Eq. (6) for u together with Eq. (11), we derive the recombination coefficient:

$$K_r = k_2n_s^2/u_s^2 = (s_0\mu\ \exp(2(Q_s - E_c)/kT)/K_{s_0}^2, \quad (12)$$

which coincides with Pick and Sonnenberg's recombination coefficient [5]. It should be mentioned that Eq. (12) is derived for a low surface coverage. Using Eq. (10) and assuming $E_c = 0$, we can derive the recombination coefficient for a metal with a clean surface

$$K_r^{clean} = (6D_0\lambda^2/g)\exp(2Q_s/kT). \quad (13)$$

Eq. (13) or, more simple expression $K_r^{clean} \approx D_0\lambda^2\exp(2Q_s/kT)$, can be useful for the estimation of the recombination coefficient on a clean metal surface.

1.4. Permeation

1.4.1. Diffusion-limited regime

The hydrogen isotope permeation is important from the point of view of the safety of thermonuclear reactors. For the first wall materials, the endothermic metals are usually used. For the metal with $Q_s > 0$, the hydrogen concentration on the front side of the sample in contact with gas is usually much higher than that on the back side ($u_0 = u_s \gg u_L$) and the permeation flux, J_L, is usually much smaller than the desorption flux ($J_L \ll J_0$). Therefore, at steady state the desorption flux, J_0, is almost equal to the flux of hydrogen sticking to the surface from the gas, J_1,

$$J_0 \cong J_1 = 2sI_0(1 - n_s/n_m)^2 \text{ (atoms/m}^2 \text{ s)}, \quad (14)$$

while the permeation flux is given by Fick's law for diffusion as

$$J_L = J_d = D(u_0 - u_L)/L \text{ (atoms/m}^2 \text{ s)}. \quad (15)$$

For $u_0 \gg u_L$, Eq. (15) reduces to

$$J_L = J_d = Du_0/L, \tag{16}$$

or, using Eq. (6) for the concentration of dissolved gas $u_0 = u_s$, the permeation flux is

$$J_L^{\text{gas}} = (D/L)\exp(-Q_s/kT)\sqrt{s_0 I_0/\nu\lambda^4}. \tag{17}$$

Finally, taking $\nu\lambda^4$ from Eq. (8): $\nu\lambda^4 = s_0\mu/K_{s_0}^2$, we can write Eq. (17) in the following form:

$$J_L^{\text{gas}} = (P/L)\sqrt{p}, \tag{18}$$

where the quantity $P = DK_s$ is defined as the permeability of the material. Eq. (18) is known as Richardson's law [10].

1.4.2. Surface-limited regime

Eq. (15) is valid if diffusion through the solid is the rate limiting factor: for a thick sample at a sufficiently high pressure, permeation will be diffusion-limited. Conversely, oxidized or contaminated of metal surface tends to enhance the importance of the surface effects. Furthermore, if the thickness of a metal or the pressure of gas in contact with the metal is reduced sufficiently, the permeation rate will tend to that of the surface-limited condition. In this case, using the recombination coefficient on the inlet K_r^0 and on the outlet K_r^L sides, the balance of fluxes near the interface between gas and metal can be written in the following form:

$$2s^0 I_0 - 2K_r^0 u_0^2 + D(u_L - u_0)/L = 0, \tag{19}$$

$$-2K_r^L u_L^2 - D(u_L - u_0)/L = 0, \tag{20}$$

$$J_L = 2K_r^L u_L^2. \tag{21}$$

Solving the system of equations (19)–(21) and taking into account that $K_r^{0,L} = s^{0,L}\mu/K_s^2$, we find

$$J_L/J_L^{\text{gas}} = \sqrt{1 - J_L/2s^0 I_0} - \sqrt{s^0/s^L}\sqrt{J_L/2s^0 I_0}, \tag{22}$$

where $J_L^{\text{gas}} = (DK_s/L)\sqrt{p}$.

2. Interaction of hydrogen atoms with metal

2.1. Inventory

It has been established experimentally [11–16] and explained theoretically [17–19] that the molecular hydrogen adsorption is often activated. On the other hand, atomic hydrogen can be easily adsorbed on the metal surface and even absorbed beneath the surface [11,12,14,16]. Fast hydrogen atoms have enough energy to penetrate into the bulk of the metal without thermalization at the surface. In many practical situations, the particular case when the projected range of implanted hydrogen is much smaller than the diffusion length ($R_p \ll L_D \approx \sqrt{Dt}$), is of interest. This situation arises, for example, under conditions of implantation of low-energy ions or atoms in the thick membrane.

Assuming that the atomic flux I_0 penetrating the metal slows down just beneath the surface, the balance of particles near the inlet surface layer is given by the following equations:

$$-2k_2 n^2 - k_3 n + k_4 u(1 - n/n_m) = 0, \tag{23}$$

$$k_3 n - k_4 u(1 - n/n_m) + I_0 = 0. \tag{24}$$

From Eqs. (23) and (24), the hydrogen concentration, n, on the surface is

$$n_{at} = \sqrt{I_0/2k_2}, \tag{25}$$

and the hydrogen concentration, u, in the absorption state in the bulk of the metal is

$$u_{at} = (k_3 n_{at} + I_0)/(k_4(1 - n_{at}/n_m)). \tag{26}$$

Comparing the expression $k_3 n_{at} = \exp((E_c - E_s)/kT)\sqrt{I_0\nu/\lambda^2}$ with I_0, for any reasonable values of E_c and E_s, for $I_0 = 10^{16}$–10^{22} atoms/m^2 s, $K_{s_0} \approx 10^{23}$ (atoms/m^3 Pa$^{1/2}$) and in the temperature range from 400 to 1000 K, we can state that $k_3 n_{at}$ is much higher than I_0. Therefore, on the assumptions that $k_3 n_{at} \gg I_0$ and $n_{at} \ll n_m$, Eq. (26) can be reduced to

$$u_{at} = \exp((E_c - Q_s)/kT)\sqrt{I_0/(2\nu\lambda^4)}, \tag{27}$$

and, using Eq. (8) for $\nu\lambda^4$, we have

$$u_{at} = K_s\sqrt{I_0/(2s\mu)}, \tag{28}$$

where K_s is Sieverts' constant and $s = s_0\exp(-E_c/kT)$ is the sticking coefficient.

2.2. Permeation

For the diffusion-limited regime, the steady-state permeation flux is defined by Eq. (16). Taking u_0 from Eq. (28), we define the permeation of hydrogen atoms through an endothermic metal ($Q_s > 0$) as

$$J_L^{\text{at}} = (DK_s/L)\sqrt{I_0/2s\mu} \tag{29}$$

or

$$J_L^{\text{at}} = (P/L)\exp(E_c/kT)\sqrt{I_0/2s_0\mu}, \tag{30}$$

where $P = DK_s$ is the same as in the case of the gas-driven permeation.

2.3. Recombination coefficient

The recombination coefficient for the atom–metal interaction is

$$K_r^{at} = I_0/2u_{at}^2 = (s_0\mu\exp(2(Q_s - E_c)/kT)/K_{s_0}^2 = s\mu/K_s^2 \quad (31)$$

and coincides with the recombination coefficient deduced for the gas–metal interaction.

2.4. Baskes' model

It is easy to find the permeation flux through the symmetrical membrane, using Baskes' model [4]. According to [4], the recombination coefficient is

$$K_B = 2s_0\mu\exp((2Q_s - E_x)/kT)/K_{s_0}^2 \quad (\mathrm{m^4\ molecules/atoms^2\ s}), \quad (32)$$

where $E_x = Q_s + E_m$ if $Q_s + E_m > 0$ and $E_x = 0$ otherwise, and s_0 is the initial zero-coverage, zero-barrier sticking coefficient. In [4] it was assumed that the desorption flux is equal to the incident flux $J_0 = I_0$. So, using (11) together with (32), we can derive the hydrogen concentration near the inlet surface for Baskes' model

$$u_0^B = \sqrt{I_0/2K_B} \quad (\mathrm{atoms/m^3}). \quad (33)$$

For the diffusion-limited regime, the permeation flux is defined by the diffusion flux $J_L = Du_0/L$ and is given in Baskes' approximation by

$$J_L^B = (D/L)\sqrt{I_0/2K_B}. \quad (34)$$

Finally, using Eqs. (32) and (34), the permeation flux according to Baskes' model is

$$J_L^B = (P/L)\sqrt{I_0/4s_0\mu}\exp(E_x/2kT)\ (\mathrm{atoms/m^2\ s}), \quad (35)$$

where $E_x = Q_s + E_m$ for endothermic metals.

Comparison of Eq. (30) with Eq. (35) shows that Baskes' permeation J_L^B through the endothermic metal by a factor of $J_L^B/J_L^{at} = \exp((Q_s + E_m)/2 - E_c)/kT)/\sqrt{2}$ differs from the permeation J_L^{at} deduced from the dissociative chemisorption model. Even for a perfectly clean surface, when the activation energy for chemisorption is zero ($E_c = 0$), there is the difference between J_L^B and J_L^{at}.

3. Interaction of fast hydrogen ions with metal

High-energy hydrogen ions can penetrate into the metal to a depth of a hundred atomic layers. If the penetration depth is comparable with the diffusion length, the expressions derived above for the diffusion-limited regime become invalid. In this case, the distribution of hydrogen atoms in the bulk of the metal should be taken into account. The ion source distribution $\varphi(x)$ can be approximated by a Gaussian-function

$$\varphi(x) = A\exp\left(-(x - R_p)^2/(2\langle\Delta x^2\rangle)\right), \quad (36)$$

where $A = 1/\int_0^L \exp(-(x - R_p)^2/(2\langle\Delta x^2\rangle))\mathrm{d}x$, R_p is the ion projected range, and $\langle\Delta x^2\rangle$ is the variance. However, in order to simplify the calculations, we assume

$$\varphi(x) = \delta(x - R_p). \quad (37)$$

In the steady state, the net of fluxes is equal to zero [20]

$$2K_r^0u_0^2 + 2K_r^Lu_L^2 = I_0, \quad (38)$$

$$2K_r^0u_0^2 = D(u_p - u_0)/R_p, \quad (39)$$

$$2K_r^Lu_L^2 = D(u_p - u_L)/(L - R_p), \quad (40)$$

where u_p and u_0 and u_L are the maximum hydrogen concentration on the depth R_p and hydrogen concentrations on inlet and outlet sides, respectively, I_0 is the incoming ion flux, D is the diffusion coefficient, L is the thickness of the metal and $K_r^{0,L} = s^{0,L}\mu/K_s^2$ (molecules atoms^{-2} m^4 s^{-1}) is the recombination coefficient on inlet and outlet sides, respectively. The desorption flux is $J_0 = 2K_r^0u_0^2$ (atom m^{-2} s^{-1}) while the permeation flux is

$$J_L = 2K_r^Lu_L^2 \ (\mathrm{atom/m^2\ s}). \quad (41)$$

Solving the system of equations (38)–(41), we have

$$J_L/J_L^{at} = \sqrt{1 - J_L/I_0} - \sqrt{K_r^0/K_r^L}\sqrt{J_L/I_0} + (R_p\sqrt{2K_r^0I_0})/D = 0, \quad (42)$$

where $J_L^{at} = (D/L)\sqrt{I_0/2K_r^0}$.

Eq. (42) can be reduced to

$$ax^4 + bx^3 + cx^2 - dx + e = 0, \quad (43)$$

where $J_L = x^2$, $a = 2K_r^0K_r^LL^2/D^2$, $b = 2K_r^0\sqrt{2K_r^L}L/D$, $c = (K_r^0 - 4LR_pI_0K_r^0K_r^L/D^2 + K_r^L)$, $d = 2R_pI_0\sqrt{2K_r^LK_r^0}/D$ and $e = 2R_p^2I_0^2K_r^0K_r^L/D^2 - K_r^LI_0$.

For endothermic metals ($Q_s > 0$), the permeation flux is usually much less than the incoming flux ($I_0 \gg J_L$). In this case, Eq. (42) can be reduced to

$$J_L^{ion} = \left(D^2/\left(8K_r^LL^2\right)\right) \times \left(\sqrt{1 + \left(8K_r^LL/D^2\right)\left(D\sqrt{I_0}/\sqrt{2K_r^0} + R_pI_0\right)} - 1\right)^2, \quad (44)$$

or, using the expression (12) for the recombination coefficient, we define the steady-state permeation flux as a function of inlet, s^0, and outlet, s^L, sticking coefficients

$$J_L^{\text{ion}} = \left(D^2K_s^2/\left(8s^L\mu L^2\right)\right) \times \left(\sqrt{1+\left(8s^L\mu L/D^2K_s^2\right)\left(DK_s\sqrt{I_0}/\sqrt{2s^0\mu}+R_pI_0\right)}-1\right)^2. \quad (45)$$

For the same sticking coefficients on both sides ($s^0 = s^L$) and the large thickness of the metal and not high temperature, the permeation flux is a function only of the surface condition on the plasma-facing (inlet) side:

$$J_L^{\text{ion}} = (DK_s/L)\sqrt{I_0/2s^0\mu} + R_pI_0/L. \quad (46)$$

If the diffusion length is larger than the ion range, Eq. (46) transforms in Eq. (29).

4. Permeation through multi-layer metal in the diffusion-limited regime

For a composite sample consisting of two or more layers of uniform thickness $L_1, L_2, \ldots, L_n$ with permeabilities $P_1, P_2, \ldots, P_n$, it is convenient to describe the behavior of the system in terms of the 'permeation resistance' [21]. The gas-permeation rate for a multi-layer sample may be written as

$$J_L^{\text{gas}} = \left(\sum_i L_i/P_i\right)^{-1} p^{1/2}, \quad (47)$$

where L_i is the thickness of the ith layer, $P_i = D_iK_{si}$ the permeability of i layer and p is the pressure on the inlet side.

For the case of the atom–metal interaction, the permeation flux through a multi-layer membrane may be written as

$$J_L^{\text{at}} = \left(\sum_i L_i/P_i\right)^{-1} \sqrt{I_0/2s\mu}, \quad (48)$$

where I_0 is the incoming atomic flux and s is the sticking coefficient on the inlet side ($s = s^0$).

Part II. Validity of the model: experimental results

5. Comparison of the gas- and atom-driven permeation and uptake in the diffusion-limited regime

It is convenient to write here the steady-state permeation, J_L, and hydrogen concentrations in the chemisorption state, n, and in the absorption state, u, for the gas–metal and atom–metal interactions for a diffusion-limited regime

$$J_L^{\text{gas}} = (P/L)\sqrt{I_0/\mu}, \quad (49)$$

$$J_L^{\text{at}} = (P/L)\sqrt{I_0/2s\mu}, \quad (50)$$

$$n_s = \lambda K_{s_0}\exp(-Q_c/kT)\sqrt{I_0/\mu}, \quad (51)$$

$$n_{\text{at}} = \lambda K_{s_0}\exp(-Q_c/kT)\sqrt{I_0/2s\mu}, \quad (52)$$

$$u_s = K_s\sqrt{I_0/\mu}, \quad (53)$$

$$u_{\text{at}} = K_s\sqrt{I_0/2s\mu}, \quad (54)$$

where $P = DK_s$ is the permeability, $\mu = 1/\sqrt{2\pi mkT}$, and $s = s_0\exp(-2E_c/kT)$ is the sticking coefficient. At present, regarding the sticking coefficient it is known that:

- Most chemisorptions on clean metal surfaces are non-activated ($E_c = 0$).
- The activation energy for chemisorption, E_c, drastically depends on the presence of contaminants.
- When pure transition metals are compared, the chemical nature of the metal seems to have a smaller influence on s_0 than its structural properties.
- For a clean surface, the sticking probability $s = s_0$ is a function of two factors: (i) the structure of the surface (i.e. whether the solid is a single crystal) and (ii) the crystallographic orientation of the surface.
- Impurities like O, S or C lower s_0.
- The pre-exponential factor s_0 of the sticking coefficient increases with the increase of the roughness factor σ. For simplicity, we consider an ideal surface with $\sigma = 1$.

Causey and Baskes [22] measured the gas-driven permeation and the plasma-driven permeation of deuterium through nickel (Fig. 2). The data were obtained for two different amounts of carbon on the nickel

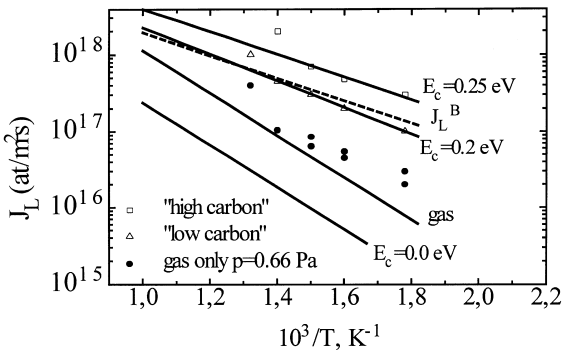

Fig. 2. The gas-driven (solid symbols) and plasma-driven (open symbols) permeation flux of deuterium through nickel as a function of temperature. The experimental data were taken from [22]. The deuterium pressure is $p = 0.66$ Pa, the ion flux of 100 eV deuterium is $I_0 = 3\times10^{20}$ D/m^2 s, the membrane thickness is $L = 3\times10^{-4}$ m. Calculated values are shown as solid lines. The deuterium permeation flux calculated by Baskes' model J_L^B is shown as dotted lines for comparison.

surface: the 'low carbon' surface had less 10% C and the 'high carbon' surface had 30% C. The calculations were performed using Eqs. (49)–(54). The data of diffusivity and solubility of deuterium in nickel [23,24] are presented in Table 1. As a pre-factor of the sticking coefficient, the value of $s_0 \leqslant 0.1$ evaluated by Eq. (10) is used which seems to be reliable [25–37] (see Table 2).

The comparison of the experimental data for the plasma-driven permeation with the theoretical expression (50) allows the activation energy for chemisorption E_c to be determined. The agreement between calculations and experimental data is quite good for the surface barrier $E_c = 0.2$ eV for 'low carbon' and $E_c = 0.25$ eV for 'high carbon' surfaces (Fig. 2). In general, the presence of impurities on the metal surface enhances E_c. Due to the presence of even small amount of contamination on the inlet surface, the sticking coefficient, s, significantly decreases and, from this, the atom-driven uptake in and permeation through the metal increase. On the other hand, the presence of impurities on the inlet surface does not influence the gas-driven processes for endothermic metals.

For a clean nickel surface ($E_c = 0.0$ eV), the atom-driven concentration in the bulk, u_{at}, increases with

Table 1
Data of hydrogen isotope diffusivity and solubility

Metal	Diffusivity		Solubility		Ref.
	D_0 (m^2/s)	E_m (eV)	K_{s_0} (atoms/m^3 $\sqrt{\text{Pa}}$)	Q_s (eV)	
D_2-Ni	4.76×10^{-7}	0.4	4.71×10^{23}	0.15	[23,24]
D_2-Cu	6.2×10^{-7}	0.39	4.1×10^{23}	0.41	[24]
D_2-MANET	1.01×10^{-7}	0.137	3.25×10^{23}	0.276	[59]
D_2-Be	6.7×10^{-9}	0.294			[60]
T_2-Be			2.3×10^{22}	0.173	[61]
D_2-BeO	1.31×10^{-9}	1.335			[62]
BeO			9.4×10^{17}	0.8	[63]
α-Fe	3.87×10^{-8}	0.045	6.14×10^{23}	0.27	[64]

Table 2
Pre-exponential sticking factor s_0

	s_0^{exp}	Temperature (K)	Ref.
Ni(1 0 0)	0.06	287	[25]
	0.06	120	[26]
	0.1–0.15	120	[26]
	$\leqslant 10^{-2}$	300	[27]
	0.4	300	[28]
	0.25	300	[29]
	0.6	300	[30]
Ni(1 1 0)	0.96	140	[31]
	0.4	300	[32]
Ni(1 1 1)	0.05	140	[31]
	0.1	120	[33]
	0.1	287	[34]
	$\leqslant 10^{-2}$	120	[27]
Ni film	0.6–0.9	78	[35]
	0.1	300	[36]
	0.25	300	[27]
	0.3	279	[37]
Fe(1 1 0)	0.16	140	[43]
Fe(1 1 0)	0.18	200	[44]
Fe(1 0 0)	0.03	300	[45]
Fe(1 0 0)-c(2 × 2)C (carbon)	10^{-3}	200	[45]
Fe(1 0 0)-p(2 × 2)O (oxygen)	10^{-4}	200	[45]
Cu	<0.1		[65,66]

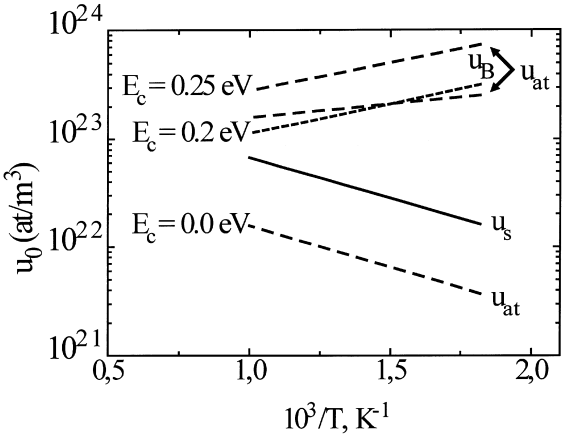

Fig. 3. The gas-driven u_s (—) and plasma-driven u_{at} (– – –) deuterium concentration just beneath the surface in nickel as a function of temperature calculated for various activation energies for chemisorption E_c. The deuterium concentration calculated by Baskes' model u_B is shown as dotted lines for comparison.

temperature, while, for a dirty surface ($E_c \geqslant 0.2$ eV), u_{at} decreases (Fig. 3). It should be noted that u_{at} increases with temperature when $E_c < |Q_s|$ and decreases when $E_c > |Q_s|$ (see Eq. (54)). The atom-driven permeation flux, J_L^{at}, can also increase and decrease with temperature depending on the surface contamination. As follows from Eq. (50), J_L^{at} increases when $E_c < |Q_s + E_m|$ and decreases when $E_c > |Q_s + E_m|$.

Although the incident molecular flux $I_0 \approx 3 \times 10^{22}$ (atoms/m^2 s) at pressure $p = 0.66$ Pa is two orders of magnitude higher than the atomic flux $I_0 = 3 \times 10^{20}$ (atoms/m^2 s), the gas-driven permeation and uptake are lower than in the case for the atomic-driven ones (Figs. 2 and 3) because of the presence of impurities on the surface which reduce J_L^{at} in the last case. For a perfectly clean surface ($E_c = 0$), gas-driven permeation and inventory are higher than the atom-driven ones.

For comparison, the permeation flux J_L^B (35) and concentration in the bulk u_B (33) based on Baskes' model are also shown in Figs. 2 and 3, respectively. According to Baskes' model, the permeation and uptake do not vary with surface contamination. This is in disagreement with experimental data, which are very sensitive to the surface composition.

Taking into account the uncertainties involved in the measurements, the agreement of experimental data with the results of calculations by Eqs. (49)–(54) is excellent.

6. Recombination and sticking coefficients

As it was derived above, the recombination coefficient, $K_r = s\mu/K_s^2$, is the same for atom- and gas-driven processes. According to Eq. (12), K_r can be written in the following form:

$$K_r = K_0 \exp(-E_r/kT), \tag{55}$$

where

$$K_0 = s_0\mu/K_{s_0}^2 \tag{56}$$

and

$$E_r = 2(E_c - Q_s). \tag{57}$$

Knowing the sticking coefficient $s = s_0 \exp(-2E_c/kT)$, we can define the recombination coefficient. Fig. 4 shows the recombination coefficient for both 'low carbon' and 'high carbon' nickel surfaces. The increase of E_c (or the increase of the amounts of carbon on the surface) results in the reduction of the recombination coefficient. The recombination coefficient has a maximum value for a clean metal surface without surface barrier ($E_c = 0.0$ eV). From Eq. (13), the recombination pre-factor for a clean surface is $K_0 \approx D_0\lambda^2 \approx 10^{-26}$ (m^4/s).

From Eqs. (55)–(57) it is clear that the recombination coefficient decreases at $E_c < |Q_s|$ and enhances at $E_c > |Q_s|$ (increase the impurities on the surface) with the increase of the temperature (Fig. 4).

According to [38], the recombination pre-factor K_0 is

$$K_0 = \nu n_m/u_m^2, \tag{58}$$

where $\nu \approx 10^{13}$ (s^{-1}) [39,40] is the vibration frequency of hydrogen, $n_m \approx 10^{19}$ (atoms/m^2) and $u_m \approx 10^{29}$ (atoms/m^3) are the maximum available concentrations on the surface and in the bulk, respectively. Then, the pre-factor of the recombination coefficient can be evaluated as $K_0 \approx 10^{26}$ (m^4/s) which is the same as that one estimated by Eq. (13).

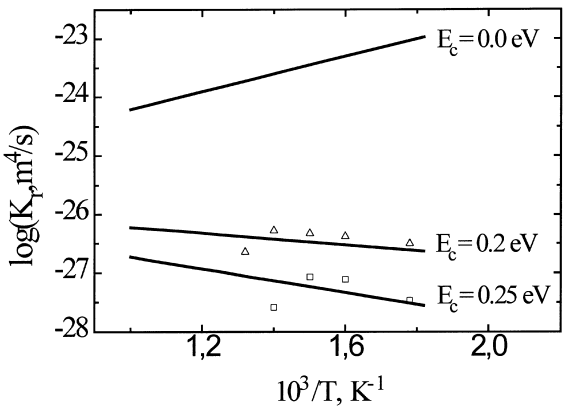

Fig. 4. The recombination coefficient of deuterium on nickel as a function of temperature calculated for various activation energies for chemisorption E_c. Calculated values are shown as lines, while experimental values taken from [22] as open symbols.

The pre-factor of the recombination coefficient was measured by Nagasaki $K_0^{Ni} = 1.5 \times 10^{-25}$ (m^4/s) for nickel [41] and by Wampler $K_0^{Fe} = 1.2 \times 10^{-29}$ (m^4/s) for iron [42]. Consequently, following Eq. (56), the sticking pre-factors are $(s_0^{Ni})^{Nag} \approx 0.5$ for nickel and $(s_0^{Fe})^{Wam} \approx 7 \times 10^{-5}$ for iron, respectively. The values of $s_0^{Ni} = 0.1$–0.9 for Ni film were measured in sorption/desorption experiments [35–37] (Table 2) and correspond to the calculated one. However, the values of $s_0^{Fe} = 0.16$–0.18 for iron were measured in sorption/desorption experiments [43,44] and are about four orders of magnitude higher than the calculated one from Wampler's experiment. The observed discrepancy may be due to influence of impurities on the surface: the value of s_0 for Fe ranges from 10^{-5} to 1 depending on the surface cleanness [45,46]. Adlayers of carbon, oxygen or sulfur may result in restrictive geometric alignment [47] which could account for the decrease in the sticking probability of hydrogen on contaminated surface.

Other possible explanation of the observed disagreement may be in different crystallographic orientation of the surface. On the (1 1 1) faces of the fcc metals (Ni) and on the (1 1 0) faces of the bcc metals (Fe) there is the general trend that small s have been reported in the past [32]. The situation is different for crystallographically more 'open' surfaces, namely, the (1 1 0) faces of the fcc and (2 1 1) faces of the bcc system. For these surfaces, the sticking probability is close to unity.

For iron and nickel, the sticking pre-factor, s_0, (and, consequently, K_0) differs by about four orders of magnitude. The sticking pre-exponential factor, s_0, is the probability that a molecule or atom which possesses the necessary activation energy and collides with a vacant surface site, is adsorbed on the surface. This factor depends on the vibrational (and also rotational and translational) modes of the molecular activated complex (adsorbed molecule and metal atoms) on the metal surface and can be calculated, for example, by the statistical partition functions [48]. As observed elsewhere [49], the nickel pre-exponential factor of the sticking coefficient is consistent with atoms recombining into molecules which have their full degrees of translational and rotational freedom, whereas the iron pre-factor is consistent with an immobile precursor state in which the molecule has no degrees of freedom than a bound atom. According to [48], for diatomic molecules, forming an immobile transition complex, we can put $s_0 \approx 10^{-4}$–10^{-2} (for example, α-Fe) and, forming a mobile transition complex $s_0 \approx 0.1$–1 (for example, Ni). Our estimations by Eq. (10) for a clean surfaces of Ni and Fe show that $(s_0^{Ni})^{calc} \approx 10^{-1}$ for nickel and $(s_0^{Fe})^{calc} \approx 10^{-2}$ for iron which is in agreement with [48].

In contrast to Pick and Sonnenberg's conclusion [5] that there is no difference between molecular and atomic hydrogen interaction with solid in the case of non-activated sorption, we state that even in the case $E_c = 0$, the pre-exponential sticking coefficient, s_0, can be considerably less than unity and enhances the plasma-driven uptake and permeation compared to the gas-driven ones.

7. Ion-driven permeation

Let us consider the plasma-driven permeation experiments for nickel and copper performed by Nagasaki et al. [50,41] and by Wilson et al. [51].

Fig. 5 shows the ion-driven permeation flux as a function of temperature measured for Ni and Cu. The agreement between the results of calculations and experimental data is quite good for the surface barrier $E_c = 0.0$ eV for Ni and $E_c = 0.32$ eV for Cu in the experiment of Nagasaki et al. [50,41], respectively, and $E_c = 0.41$ eV for Cu in the experiment of Wilson et al. [51]. It seems, that in the experiment of Wilson, the copper surface was more dirty than in the experiment of Nagasaki.

The adsorption of hydrogen isotope on nickel does not seem to require an activation energy. A small activation barrier about 0.05 eV was reported in [28]. In contrast to the case of nickel, copper has a significant activation barrier for hydrogen isotope chemisorption [11,52] that is in good agreement with our results. In general, adsorption of hydrogen at d-metal surface, e.g.

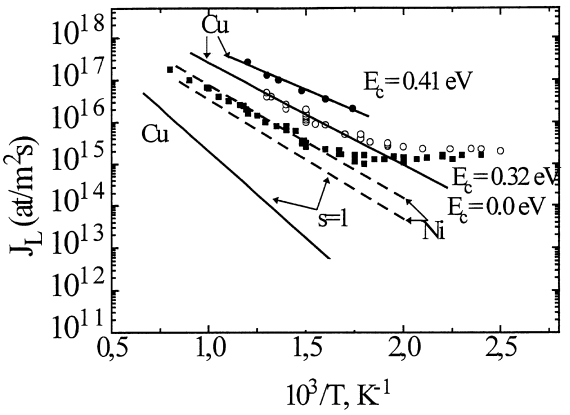

Fig. 5. The ion-driven deuterium permeation flux through nickel and copper as a function of temperature. The experimental data for Ni are taken from [50] and for Cu from [41,51]. In the experiments of Nagasaki et al. the ion flux ($I_0 = 1.1 \times 10^{19}$ (D/m^2 s)) and the membrane thickness ($L = 1.2 \times 10^{-4}$ m) for Ni [50] are similar to those for Cu ($I_0 = 1 \times 10^{19}$ (D/m^2 s) and $L = 1.3 \times 10^{-4}$ m) [41]. The experimental conditions of Wilson et al. for Cu [51] are the following: $I_0 = 1 \times 10^{20}$ (D/m^2 s) and $L = 5.1 \times 10^{-4}$ m. Calculated by Eq. (46) values are shown as dashed lines for Ni and as solid lines for Cu.

Ni, is non-activated or only slightly activated with barrier less than 0.1 eV, whereas at *s*-metal surfaces such as Cu, Al, Be the value of E_c is considerably higher ranging from 0.3 to 1 eV.

From Fig. 5 it follows that the permeation flux through nickel is lower than through copper. For the gas-permeation experiment, the permeation flux through nickel is higher than through copper (see curves for $s = 1$ in Fig. 5). We can conclude that from results of the gas-driven experiment, it is not possible to predict the plasma-driven permeation and uptake.

An issue to be considered is the influence of the ion range R_p on the permeation flux J_L^{ion} (Fig. 6).

The influence of the ion range on the permeation through the endothermic metal ($Q_s > 0$) depends on the following factors: the thickness of the sample L, the diffusion coefficient of hydrogen in the metal D, the value of the incident flux I_0, and the conditions on the surface. The smaller the thickness of the membrane, the higher the diffusion coefficient, the higher the energy of implanted particles or the higher the activation energy for chemisorption E_c on one of the metal sides, the more significant is the influence of the ion range on the permeation flux. A good agreement of calculations by Eq. (46) with experiments is obtained for $R_p = 2 \times 10^{-8}$ m for copper and $R_p = 1 \times 10^{-8}$ m for nickel. The influence of the ion range tends to increase the permeation flux at low temperature ($T < 500$ K). But at high temperature, since diffusion is a very fast process and the diffusion length becomes much larger that the ion range ($L_D \approx \sqrt{Dt} \gg R_p$), the implantation depth does not significantly affect the permeation.

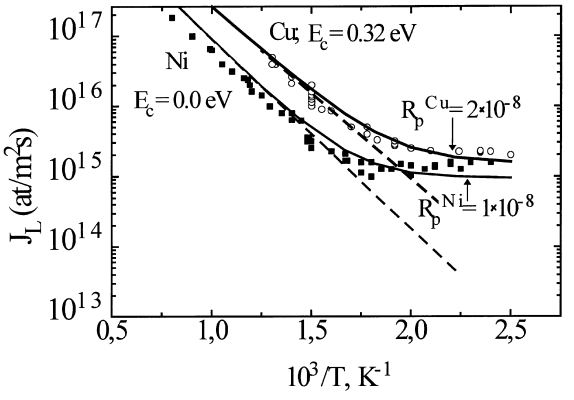

Fig. 6. The plasma-driven deuterium permeation flux through Ni [50] (■) and Cu [41] (○) as a function of temperature. Calculated by Eq. (46) values are shown as lines at various ion range R_p. Dashed lines: $R_p = 2 \times 10^{-10}$ m. Solid lines: $R_p^{Ni} = 1 \times 10^{-8}$ m for Ni and $R_p^{Cu} = 2 \times 10^{-8}$ m for Cu.

Part III. Assessment of the tritium permeation through multi-layer metal

8. Influence of various coatings on the tritium permeation through MANET

From the point of view of safety of thermonuclear reactors, it is important to know how the different coatings affect the hydrogen isotope permeation. For example, it was assumed that the first wall between the plasma and the coolant represents the martensitic 7–10% Cr steel such as T91, F82H, MANET or Batman of thickness 3 mm (water cooled led lithium blanket) [53] or 5 mm (helium cooled pebble bed blanket) [54]. For our assessment, MANET (Martensitic steel DIN 1.4914 for NET) of the thickness $L^{MAN} = 5$ mm is used as reference. The thickness of Be and Cu layers is the same and equals to $L^{Cu,Be} = 1$ mm. The thickness of BeO is $L^{BeO} = 8 \times 10^{-3}$ mm. The tritium ion flux is evaluated as $I_0 = 1.5 \times 10^{20}$ (atoms/m^2 s) [55]. The data of hydrogen isotope solubility and diffusivity are given in Table 1. The hydrogen isotope extrapolated values for diffusivity are defined using the classical diffusion theory $D_i/D_j = \sqrt{m_j/m_i}$, where i and j are two different hydrogen isotopes.

For the diffusion-limited regime, only the inlet sticking coefficient, s, influences the permeation flux. The sticking coefficients for various bare metals are presented in Table 3. It is worth noting that values of s presented in Table 3 are only rough approximations. The surface impurities create the activation barrier for chemisorption which considerably decreases the sticking coefficient s. As a result, for the same metal, s can vary greatly with surface composition. As it was mentioned above, the crystallographic orientation of the surface and the surface structure also change the value of s. As it was reported in [39], the experimentally determined recombination coefficient and, consequently, the sticking coefficient, range about five orders of magnitude for Fe, six for Ni, four for Pd, and six for stainless steel.

It appears that the surface may be cleaned or modified in some way by the energetic particles [56]. The sticking coefficient for such an extremely clean surface is often close to unity ($s \cong 1$) [57,58]. Fig. 7 shows the influence of various coatings on the tritium permeation

Table 3
Sticking coefficient

Metal	Sticking coefficient	Ref.
MANET	$5 \times 10^{-6} \exp(-0.198/kT)$	[59]
Be	$3 \times 10^{-7} \exp(-0.626/kT)$	[67]
BeO	$2.12 \times 10^{-19} \exp(-2.18/kT)$	[68]
Cu	$0.08 \exp(-0.64/kT)$	This work
Ni	0.08	This work

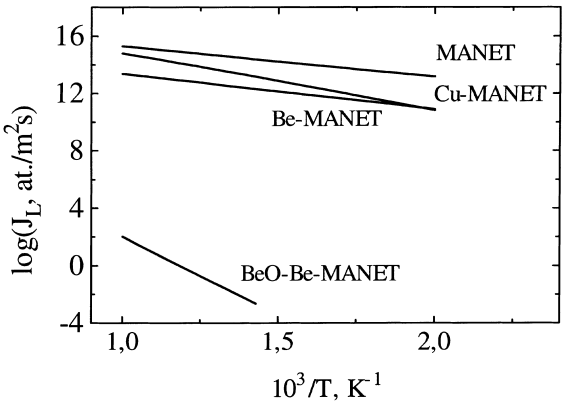

Fig. 7. The atom-driven tritium permeation through a bare MANET and MANET with Cu, Be and BeO–Be coatings as a function of temperature for a clean inlet surface ($s = 1$).

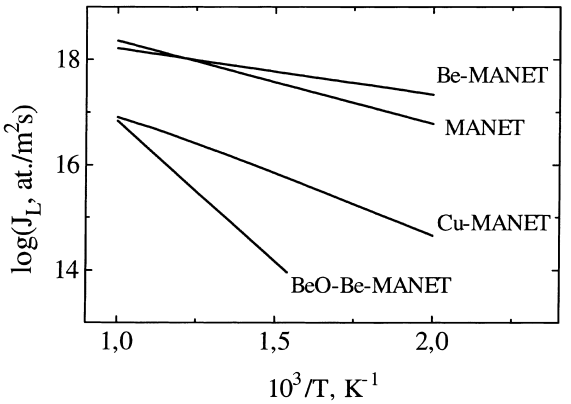

Fig. 8. The atom-driven tritium permeation through a bare MANET and MANET with Cu, Be and BeO–Be coatings as a function of temperature using the sticking probability, s, presented in Table 3.

through MANET for perfectly clean plasma-facing surfaces. The atom-driven permeation, J_L^{at}, through BeO–Be-MANET is appreciably lower than that for a bare MANET. The presence of BeO on the plasma-facing side results in nineteen orders of magnitude of the reduction in the tritium permeation. Be and Cu coatings have smaller effects on the permeation behavior of MANET: Be coating decreases the tritium permeation by two and Cu coating by one orders of magnitude (Table 4). However, the different situation arises when we consider bare (presence of small amount of contamination) surfaces (Fig. 8). Using the sticking coefficients presented in Table 3, we see that Be coating can result in *the increase* of the tritium permeation compared to bare MANET! This is obvious if we consider Eq. (32): $J_L^{at} = \sum (L_i/P_i)^{-1} \sqrt{I_0/2s\mu}$. For a perfectly clean plasma-facing surface ($s = 1$), the permeation flux, J_L^{at}, through a multi-layer target depends only on the permeabilities, P_i, of metals contained in the target. Due to the permeability for Cu, Be and BeO being lower than that for MANET (Fig. 9), these metals can work as a permeation barrier if the plasma-facing side will be sputter-cleaned during plasma operation. For unclean surfaces, the sticking coefficient, s, is less than unity. With the reduction of s, the atom-driven permeation flux, J_L^{at}, increases: $J_L^{at} \approx 1/\sqrt{s}$. The sticking probability for MANET is higher than that for Be: $s^{MANET} \gg s^{Be}$. From this, the permeation through bare MANET can be less than that through Be with usual (unclean) surface. Due to the fact that $s^{Cu} > s^{MANET}$ and $P^{Cu} < P^{MANET}$, the permeation flux through Cu is two orders of magnitude smaller than that through steel: $J_L^{Cu} < J_L^{MANET}$. Although s for BeO is much smaller than that for steel, J_L^{BeO} is smaller than J_L^{MANET} because permeabilities $P^{BeO} \ll P^{MANET}$. The permeation flux through BeO–Be-MANET with a clean plasma-facing side is much smaller than that through BeO–Be-MANET with contaminated surface (Table 4). In general, a lowest permeation flux corresponds to a highest sticking probability $s = 1$ (i.e. for a perfectly clean surface). On contaminated surface the value of the sticking coefficient can be crucial for the permeation of atomic hydrogen through the metal.

Table 4
Steady-state atom-driven permeation flux (atoms $m^{-2}\,s^{-1}$) at temperature $T = 600$ K

Metal	Unclean surface	Clean surface $s = 1$
MANET	2×10^{17}	7.5×10^{13}
Be-MANET	4.3×10^{17}	5.5×10^{11}
BeO–Be-MANET	1.9×10^{13}	6×10^{-6}
Cu-MANET	2.8×10^{15}	1.6×10^{12}

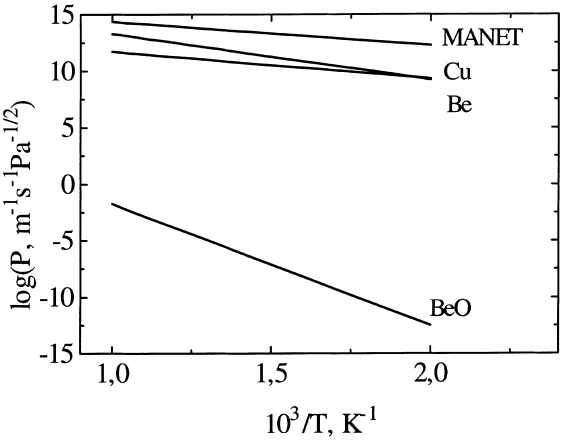

Fig. 9. The tritium permeabilities for a bare MANET, Cu, Be and BeO as a function of temperature.

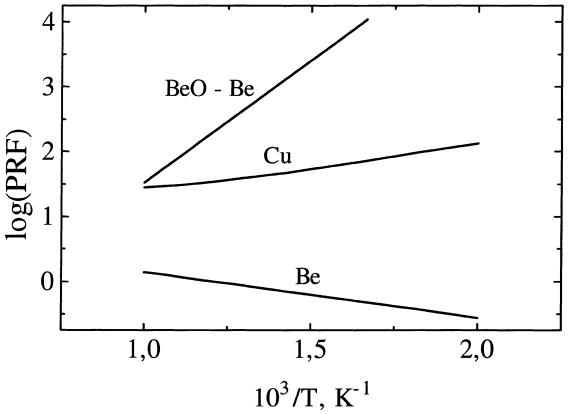

Fig. 10. The tritium PRF (permeation reduction factor) for MANET with Cu, Be and BeO–Be coatings as a function of temperature.

The permeation barrier can work differently for different temperatures: for low temperature the plasma-facing coatings decrease the tritium permeation better than for high temperature. Permeation reduction factor, PRF, defined as the ration of the tritium permeation through MANET without coating to the tritium permeation through MANET with coating, as a function of the temperature is presented in Fig. 10.

The gas-driven permeation through bare MANET and MANET with various coatings is qualitatively similar to the atom-driven permeation, J_L^{at}, through metals with clean inlet surface ($s = 1$) but qualitatively differs from J_L^{at} through the metals with usual (unclean) surface. As a result, the use of gas-driven permeation experiments in order to qualitatively predict the influence of various coatings on J_L^{at} is possible only for metals with a perfectly clean surface. In other cases, the behavior of J_L^{gas} and J_L^{at} might deviate significantly.

Conclusions

This work had three objectives. The first was to describe in detail the model for hydrogen–metal interaction. The second was to show the validity of the model by comparison with experiments. And the third was to estimate the tritium permeation through martensitic steel MANET covered by copper, beryllium and beryllium oxide in contact with tritium gas and plasma, taking into account the present knowledge about the sticking coefficient which is responsible for the influence of the surface processes on the hydrogen isotope–metal interaction.

The conclusions relating to these major objectives are as follows:

1. The dissociative chemisorption model shows a good agreement with experimental permeation data. Estimations of the recombination coefficient are in good agreement with experimental results. The model proposed by Baskes' is in disagreement with experimental measurements.
2. In the diffusion-limited regime, which takes place for the thick endothermic metal proposed to be used for the first wall of the fusion reactors, only the surface conditions on inlet side are important. The reduction of the sticking coefficient on inlet side of the metal (contaminated surface) drastically increases the atom-driven permeation through and inventory in the metal. Since the sticking coefficient is usually less than unity even for a clean surface, the atom-driven permeation and uptake are higher than the gas-driven ones for the same incident hydrogen flux.
3. The gas-driven permeation through the multi-layer membrane depends only on permeabilities of materials contained in the target, whereas the value of the sticking coefficient s on the inlet surface of the membrane can be crucial for the plasma-driven permeation. If the coating can be used as a permeation barrier for the gas-driven permeation, it does not mean that this coating can be used as the same permeation barrier for the plasma-driven permeation. To make use of the coating as a permeation barrier for the plasma–metal interaction, the knowledge of the surface composition of the coating is required.
4. Using the database about the sticking coefficient, the assessment of the steady-state permeation of tritium through a bare martensitic steel MANET and MANET coated by beryllium, beryllium oxide and copper has been done. It was shown that both Cu and BeO–Be coatings decrease the atom-driven permeation while Be coating can increase the atom-driven permeation.

The presented fitting of analytical expressions can be useful for evaluation of gas- and plasma-driven uptake and permeation.

References

[1] J.S. Wang, Proc. Cambridge Philos. Soc. 32 (1936) 657.
[2] F. Waelbroeck, I. Ali-Khan, K.J. Dietz, P. Wienhold, J. Nucl. Mater. 85&86 (1979) 345.
[3] A.I. Livshitz, Vacuum 29 (1979) 103.
[4] M.I. Baskes, J. Nucl. Mater. 92 (1980) 318.
[5] M.A. Pick, K. Sonnenberg, J. Nucl. Mater. 131 (1985) 208.
[6] P.M. Richards, J. Nucl. Mater. 152 (1988) 246.
[7] A.A. Pisarev, O.V. Ogorodnikova, J. Nucl. Mater. 248 (1997) 52.
[8] C. Zener, in: W. Shockley (Ed.), Imperfection in Nearly Perfect Crystal, Wiley, New York, 1952, p. 289.
[9] I. Ali-Khan, K.J. Dietz, F.G. Waelbroeck, P. Wienhold, J. Nucl. Mater. 76–78 (1978) 337.
[10] O.W. Richardson, Philos. Mag. 7 (1904) 266.

[11] C.S. Alexander, J. Pritchard, J. Chem. Soc. Faraday Trans. I 68 (1972) 202.
[12] F. Greuter, E.W. Plummer, Solid State Commun. 48 (1983) 37.
[13] E.M. McCash, S.F. Parker, J. Pritchard, M.A. Chesters, Surf. Sci. 215 (1989) 363.
[14] X.L. Zhou, J.M. White, B.E. Koel, Surf. Sci. 218 (1989) 201.
[15] A.G. Sault, R.J. Madix, C.T. Campbell, Surf. Sci. 169 (1986) 347.
[16] L. Stobinski, R. Dus, Surf. Sci. 269&270 (1992) 383.
[17] J. Harris, Appl. Phys. A47 (1988) 63.
[18] J. Harris, Surf. Sci. 221 (1989) 335.
[19] D. Halstead, S. Holloway, J. Chem. Phys. 93 (1990) 2859.
[20] B.L. Doyle, J. Nucl. Mater. 111&112 (1982) 628.
[21] R.A. Strehlow, H.C. Savage, J. Nucl. Mater. 53 (1974) 323.
[22] R.A. Causey, M.I. Baskes, J. Nucl. Mater. 145–147 (1987) 284.
[23] W. Eichenauer, W. Löser, H. Witte, Z. Metallkd. 56 (1965) 287.
[24] L. Katz, M. Guinan, T.J. Borg, Phys. Rev. B 4 (1971) 330.
[25] J. Lapujoulade, K.S. Neil, Surf. Sci. 35 (1973) 288.
[26] K. Christmann, Z. Naturforsch. 34a (1979) 22.
[27] A.M. Horgan, I. Dalis, Surf. Sci. 41 (1974) 624.
[28] A.V. Hamza, R.J. Madix, J. Phys. Chem. 89 (1985) 5381.
[29] K. Christmann, O. Scober, G. Ertl, M. Neumann, J. Chem. Phys. 60 (1974) 4528.
[30] S. Andersson, Chem. Phys. Lett. 55 (1) (1978) 185.
[31] A. Winkler, K.D. Rendulic, Surf. Sci. 118 (1982) 19.
[32] K. Christmann, Surf. Sci. Rep. 9 (1–3) (1988) 3.
[33] K. Christmann, R.J. Behm, G. Ertl, M.A. Van Hove, W.H. Weinberg, J. Chem. Phys. 70 (1979) 4168.
[34] J. Lapujoulade, K.S. Neil, J. Chem. Phys. 57 (8) (1972) 3535.
[35] P. Nowacki, R. Dus, Ann. Soc. Chim. Polonorum 5l (1977) 103.
[36] M. Procop, J. Völter, Z. Phys. Chem. 253 (1973) 33.
[37] D.D. Eley, P.R. Norton, Proc. Roy. Soc. London A 314 (1970) 319.
[38] S.M. Myers, P.M. Richards, W.R. Wampler, F. Besenbacher, J. Nucl. Mater. 165 (1989) 9.
[39] W. Ho, N.J. DiNardo, E.W. Plummer, J. Vac. Sci. Technol. 17 (1980) 134.
[40] P. Nordlander, S. Holloway, J.K. Norskov, Surf. Sci. 136 (1984) 59.
[41] T. Nagasaki, R. Yamada, M. Saidoh, H. Katsuta, J. Nucl. Mater. 151 (1988) 189.
[42] W.R. Wampler, J. Nucl. Mater. 313 (1987) 145.
[43] F. Bozso, G. Ertl, M. Grunze, M. Weiss, Appl. Surf. Sci. 1 (1977) 103.
[44] E.A. Kurz, J.B. Hudson, Surf. Sci. 195 (1988) 31.
[45] J. Benziger, R.J. Madix, Surf. Sci. 94 (1980) 119.
[46] P.L. Andrew, A.A. Haasz, J. Vac. Sci. Technol. A8 (3) (1990) 1807.
[47] M. Balooch, R.E. Stickney, Surf. Sci. 44 (1974) 310.
[48] D.O. Hayward, B.M.W. Trapnell, Chemisorption, Butterworths, London, 1964.
[49] P.M. Richards, S.M. Myers, W.R. Wampler, D.M. Folstaedt, J. Appl. Phys. 65 (1) (1989) 180.
[50] T. Nagasaki, R. Yamada, H. Ohno, J. Vac. Sci. Technol. A10 (1) (1992) 170.
[51] K.L. Wilson, R.A. Causey, N.I. Baskes, J. Vac. Sci. Technol. A5 (4) (1987) 2319.
[52] R.J. Mikovsky, M. Boudart, H.S. Taylor, J. Am. Chem. Soc. 76 (1954) 3814.
[53] L. Giancarli, M.A. Fütterer, Water-cooled Pb-17Li DEMO blanket line, Status Report on the related EU activities, Rapport DMT 95/505 (SERMA/LCA/1801), 1995.
[54] M. Dalle Donne, Eropean DEMO BOT Solid Breeder Blanket, KfK 5429, Nov. 1994.
[55] L. Berardinucci, M. Dalle Donne, Fusion Technol. 2 (1997) 1427.
[56] J. Winter, F. Waelbroeck, P. Wienhold, T. Schelske, J. Nucl. Mater. 111&112 (1982) 243.
[57] J.B. Taylor, I. Langmuir, Phys. Rev. 44 (1933) 423.
[58] J.K. Roberts, Proc. Roy. Soc. A 152 (1935) 445.
[59] E. Serra, A. Perujo, J. Nucl. Mater. 240 (1997) 215.
[60] E. Abramov, M.P. Riehm, D.A. Thompson, W.W. Smeltzer, J. Nucl. Mater. 175 (1990) 90.
[61] V.I. Shapovalov, Ju. Dukel'skii, Russ. Metall. 5 (1988) 201.
[62] G. Longhurst, R.A. Andrel, T.J. Dolan, M.J. Mulock, Fusion Technol. 28 (3) (1995) 1217.
[63] R.G. Macaulay-Newcombe, D.A. Thompson, J. Nucl. Mater. 212–215 (1994) 942.
[64] K.S. Forcey, I. Iordanova, D.K. Ross, Mater. Sci. Technol. 6 (1990) 357.
[65] M. Balooch, M.J. Cardillo, D.R. Miller, R.E. Stickney, Surf. Sci. 46 (1974) 358.
[66] M.J. Cardillo, M. Balooch, R. Stickney, Surf. Sci. 50 (1975) 263.
[67] G. Federici, D. Holland, J. Brooks, R. Causey, T.J. Dolan, G. Longhurst, Symposium on Fusion Engineering, Champaing, Urbana, II 30 Sept.–5 Oct. 1995.
[68] S. Cho, A.R. Raffay, M.A. Abdou, J. Nucl. Mater. 212–215 (1994) 961.